



Proceeding Paper

Numerical Analysis of Debris Impact Forces and Its Environmental Repercussions Using Smoothed Particle Hydrodynamics [†]

Muhammad Khairi A. Wahab ¹, Mohd Remy Rozainy Mohd Arif Zainol ^{1,2,*}, Mohamad Aizat Abas ³
and Norizham Abdul Razak ⁴

¹ School of Civil Engineering, Engineering Campus, Universiti Sains Malaysia, Nibong Tebal 14300, Penang, Malaysia; muhdkhairi88@gmail.com

² River Engineering and Urban Drainage Research Centre (REDAC), Engineering Campus, Universiti Sains Malaysia, Nibong Tebal 14300, Penang, Malaysia

³ School of Mechanical Engineering, Engineering Campus, Universiti Sains Malaysia, Nibong Tebal 14300, Penang, Malaysia; aizatabas@usm.my

⁴ School of Aerospace Engineering, Engineering Campus, Universiti Sains Malaysia, Nibong Tebal 14300, Penang, Malaysia; norizham@usm.my

* Correspondence: ceremony@usm.my

[†] Presented at the 6th International Conference on Green Environmental Engineering and Technology (IconGEET 2024), Bali, Indonesia, 29–30 August 2024.

Abstract: Debris flow is a destructive event occurring in elevated terrains, causing significant damage to the affected areas. It results in casualties and significant harm to the environment and society. Hence, a comprehensive evaluation is essential in order to prevent, mitigate, and increase knowledge of the consequences of debris flows. This paper focuses on evaluating the impact of the deposition board. The methodology involved a simulation of two cases to demonstrate the debris flow based on the steepness of the flume slope at 25° angles with full and half openings at the gate. The limestone particles with a total volume of $1 \times 10^3 \text{ m}^3$ acted as debris and were released with water from the tank to the deposition board with an area of 1 m^2 . The force of particle distribution from the flume that hit the building block on the deposition board was determined. Based on the numerical results, the maximum force was about 55.2 N and 47.3 N for each fully open and half open gate, respectively. In actual situations, the maximum impact force (5520 N) can be 100 times greater compared to model values (55.2 N). Research indicates that pressures over 100 kPa cause damage to reinforced concrete structures. Debris flow can pose a substantial risk to the impacted area in real-life scenarios. This study is valuable for conducting risk assessments, creating guidelines, and reducing the likelihood of debris flows in high-risk areas.

Keywords: debris flow; SPH; risk assessment; impact force; computational



Academic Editor: Sara Yasina Yusuf

Published: 13 March 2025

Citation: Wahab, M.K.A.; Zainol, M.R.R.M.A.; Abas, M.A.; Razak, N.A. Numerical Analysis of Debris Impact Forces and Its Environmental Repercussions Using Smoothed Particle Hydrodynamics. *Environ. Earth Sci. Proc.* **2025**, *33*, 7. <https://doi.org/10.3390/eesp2025033007>

Copyright: © 2025 by the authors. Licensee MDPI, Basel, Switzerland. This article is an open access article distributed under the terms and conditions of the Creative Commons Attribution (CC BY) license (<https://creativecommons.org/licenses/by/4.0/>).

1. Introduction

Debris flow is a natural phenomenon that has been observed in hilly regions with uphill valleys or streams that receive significant annual rainfall. The phenomenon is one of the most hazardous natural phenomena that impact mountainous environments due to its large volume of carried debris and extensive runoff [1]. Debris flow is a mixture of solids, soil, wood, gravel, pebbles, snow, ice, and water that moves down slopes due to gravity [2]. These occurrences often lead to significant destruction of property, loss of life, and changes in the physical features of riverbeds and mountain slopes [1,3,4].

Significant rainfall led to serious flooding and landslides in many regions of the country [5–7]. Debris flows can result from various mechanisms, including heavy rainfall that transforms landslides into rapidly moving liquid sediments [6,8–10].

Debris flow development involves three stages: initiation area, propagation zone, and deposition area [1,11]. The initiation phase involves the release of the initial large amounts. The most common type is debris flow, which is triggered by either a single huge landslide or a sequence of smaller landslides. They occur when a landslide or debris slide transitions into a debris flow. Mobilization is the transformation of a stationary mass of liquid soil, silt, or rock into debris flows. Surface-water runoff significantly contributes to the formation of a debris flow [11–15]. Debris flows can result from steep channels containing a large amount of sediment, shallow landslides, and common occurrences in high-altitude areas [16–19]. The triggered process is influenced by various parameters, such as geomorphology, geotechnical properties of slope angle, hydrological elements, and geological conditions [9,20].

Debris flows transport large amounts of sediment, which can affect water quality in rivers and streams. The introduction of sediments can lead to increased turbidity, impacting aquatic life and water usability for human consumption [21,22]. Additionally, the sediment can carry pollutants and nutrients, further degrading water quality [22]. Tuckett and Koetsier [23] found that debris flows can alter the biotic community structure in streams by affecting the availability and processing of carbon sources, which in turn influences the metabolism of aquatic ecosystems. Increased turbidity and the presence of pollutants can harm aquatic life, including fish and macroinvertebrates. The physical disturbance caused by debris flows can lead to the removal of vegetation and alteration of habitats. This disruption can favor r-strategist species—those that reproduce quickly and can exploit disturbed environments—over more sensitive species [23]. For example, amphibians and certain fish species may be particularly vulnerable to the changes brought about by debris flows. The impacts of debris flows extend beyond immediate physical destruction. For instance, the alteration of stream channels can lead to long-term changes in hydrology and sediment dynamics, affecting the ecological balance of the area. Parise and Cannon highlight that post-fire conditions can exacerbate the likelihood of debris flows, leading to a cycle of increased erosion and habitat degradation [24].

The destructive potential of debris flow is also influenced by the characteristics of the flow itself, including its density and velocity. The velocity of debris flows can vary significantly, with higher velocities resulting in greater destructive potential. Studies indicate that debris flows can reach velocities of up to 30 m/s, which can lead to substantial impact forces on structures [25–27]. Additionally, the density of the debris flow, which is affected by the composition of the materials involved, plays a crucial role in determining the flow's momentum and, consequently, its destructive force [28]. Studies have shown that the impact force can vary significantly based on the flow's composition, which may include a mixture of water, mud, and solid debris [29,30]. The variability in impact forces is compounded by the inhomogeneity of debris flow materials, which can lead to fluctuating pressures on structures over time [29]. For example, research conducted by Hu et al. [28] on the Zhouqu disaster illustrates how varying impact pressures can lead to different levels of damage to buildings, with reinforced concrete structures experiencing severe damage at pressures exceeding 100 kPa [28–31]. The vulnerability of buildings to debris flow impacts is influenced by their design and materials. Research by Kang and Kim indicates that different building types exhibit varying degrees of vulnerability based on their structural characteristics and the impact forces they experience [31]. For instance, non-concrete structures may suffer complete destruction at impact pressures exceeding 30 kPa, while concrete structures may withstand higher pressures [31]. Studying and comprehending the

causes of debris flow starting under different conditions is crucial for creating strategies to mitigate debris flow [32–34].

2. Smoothed Particle Hydrodynamics (SPH) Formulation

The SPH integral interpolation function $f(x)$ can precisely simulate continuous fluid motion using several particles with mass and momentum [35–37]. The function $f(x)$ at point (x, y, z) is estimated using the expression provided below:

$$f(x) = \int_{\Omega}^a f(x')W(x - x', h)dx' \tag{1}$$

Ω denotes the computational domain at position x , $f(x')$ is the volume element over the domain, W is the weight equation or smooth kernel function, and h is the smooth length that specifies the size of the computational domain of the kernel function.

Numerical approximations of the integrals are computed by summing the contributions from neighboring particles inside the specified region, with the subscript indicating an individual particle.

$$f(x_a) \approx \sum_b f(x_a)W(x_a - x_b, h)\Delta v_b \tag{2}$$

where Δv_b represents the volume of the neighboring particle (b), $\Delta v_b = \frac{m_b}{\rho_b}$, m is the mass, and ρ is density.

Where the subscript represents a single particle, it then becomes the following:

$$f(x_a) \approx \sum_b f(x_a) \frac{m_b}{\rho_b} W(x_a - x_b, h) \tag{3}$$

The selection of a smoothing kernel will greatly affect the performance of an SPH model. Kernel functions play a crucial role in the SPH approach, impacting its computational correctness and stability. Consequently, they have been extensively researched by numerous scholars [38–41]. According to Yang et al. [42], the stability of SPH depends on the second derivative of the kernel function. Kernels are expressed as a function of the dimensionless distance between particles (q). DualSPHysics offers two kernels: Cubic Spline and Quintic. Users can choose from these kernel definitions with flexibility.

3. Methodology

3.1. Validation of the Developed SPH Model

The accuracy of the SPH simulations was validated through a comparison between the obtained velocity data and Particle Image Velocimetry (PIV), while the shape of the deposition from SPH [38–41] was validated by comparing it with the shape observed in the experiment. The level of accuracy was assessed by considering the percentage difference for each case among the 12 cases.

Validation in numerical analysis is essential for verifying the accuracy and dependability of computational models by comparing their predictions with experimental measurements. Researchers can enhance the reliability of computational models and make well-informed decisions by integrating numerical simulations with experimental data. Specific criteria or standards are frequently used to verify the reliability and validity of findings. The criteria are used to evaluate the quality and reliability of the results. The criteria are categorized into four groups: A (<10%), B (10–30%), C (30–40%), and D (>50%). Table 1 displays the accuracy levels for each category: A for good accuracy; this category signifies good accuracy, indicating that the findings are highly reliable and valid. Results falling within this range suggest minimal error and strong confidence in the conclusions drawn

from the data. B for acceptable accuracy; findings in this range are considered to have acceptable accuracy. While there may be some degree of error, the results are still deemed reliable for practical applications and can be used to inform decisions. C for marginal accuracy; this category reflects marginal accuracy. Results within this range indicate a higher level of uncertainty, suggesting that the findings should be interpreted with caution. Researchers may need to conduct further investigations to confirm the validity of the results. Last of all, D for low accuracy; findings classified under this category are characterized by low accuracy. The high level of error suggests that the results are unreliable and may not accurately represent the underlying phenomena. Caution is advised when interpreting these findings, and further research is typically warranted [43].

Table 1. Accuracy based on relative error.

Category	Range (%)	Quality
A	<10	Good
B	10–30	Acceptable
C	30–40	Marginal
D	50>	Poor

The categorization of accuracy levels serves as a valuable tool for researchers to evaluate the quality of their findings. By applying these criteria, researchers can identify potential weaknesses in their studies and take necessary steps to enhance the reliability and validity of their results.

3.2. Experimental Setup for Debris Flow Model Test for Validation

Measuring the relevant parameters of debris flow in the field is challenging due to the catastrophic nature of these occurrences. The laboratory model test is often used to study debris flow deposition. The study’s framework consisted of three main components: a water tank, a flume, and a deposition board. The water tank was filled manually using a pump mechanism, with the flow being controlled by a butterfly valve attached to the pipe. The model’s physical dimensions were as follows: The model had dimensions of 4.55 m × 1.1 m × 1.5 m. The water tank measured 1 m × 1 m × 1 m. The flume was 2.5 m × 0.1 m × 0.01 m. The deposition board was 1 m × 1 m. The model was constructed using a 10 mm thick polyvinyl chloride (PVC) sheet. Refer to Figure 1 for a visual representation of the model’s geometry.

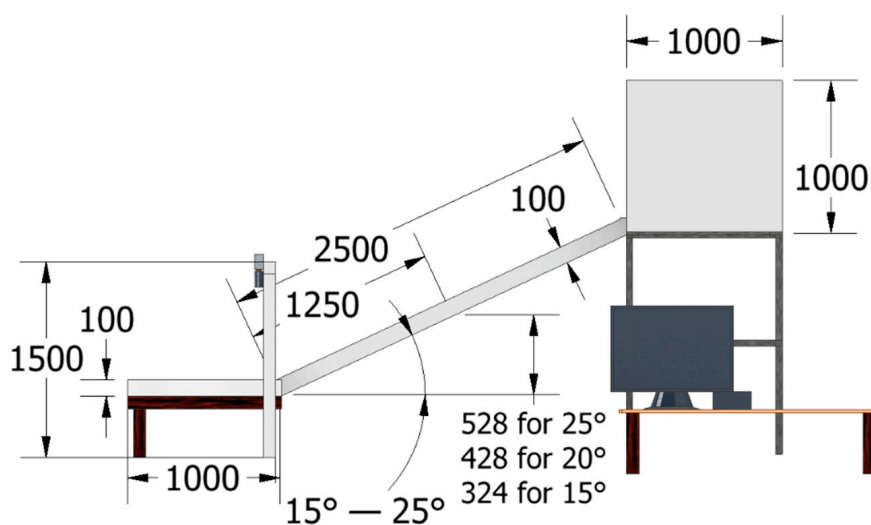


Figure 1. The geometry of the physical model with PIV setup.

The validation involved twelve cases that were exposed to different water levels, flume angles, and water gate openings. The layout of these case studies and their respective operations is detailed in Table 2, offering a thorough summary of the methods used in this section. This validation study demonstrates the effectiveness of hydrodynamic models in simulating fluid behavior under different operational scenarios. By comparing the experimental data with model predictions, the validation process assesses the accuracy of the hydrodynamic model and identifies areas for improvement [44]. The findings underscore the importance of comprehensive testing under varied conditions to enhance model reliability.

Table 2. Experiments that have been undertaken.

Case Study	Flume Degree (°)	Water Level (mm)	Gate Opening
1	15	120	Half
2	15	120	Full
3	15	150	Half
4	15	150	Full
5	20	120	Half
6	20	120	Full
7	20	150	Half
8	20	150	Full
9	25	120	Half
10	25	120	Full
11	25	150	Half
12	25	150	Full

The results of experiments and numerical analysis by comparing the deposition patterns. This process is intended to determine the similarity of their shapes. A sediment viscosity of 1.0 was incorporated into the simulation via several trial-and-error procedures within a tolerable parameter range. Approximately three numerical scenarios closely mimic the experiment’s deposition pattern out of a total of 12. Table 3 features cases, specifically Case 2, Case 8, and Case 9, which are bolded and displayed in this section. To calculate the percentage of sediment deposition in the region, subtract the plane area from the entire area of the deposition board (measured 1000 × 1000 mm or 1 × 10⁶ mm²), and then multiply the result by 100. This enables the calculation of the proportion of sediment accumulated on the sedimentation board.

Table 3. Relative error in the planar area of the numerical data compared to the experimental data.

Case No.	Planar Area (mm ²)		Relative Error (%)
	Experimental (×10 ³)	SPH (×10 ³)	
1	536.79	594.78	10.25
2	436.93	450.14	2.98
3	488.42	547.41	11.39
4	402.34	451.66	11.55
5	461.38	519.03	11.76
6	447.06	493.72	9.92
7	415.86	462.13	10.54
8	290.03	320.00	9.83
9	367.62	408.24	7.51
10	321.46	364.98	12.68
11	485.07	550.74	14.05
12	298.70	331.70	10.47

Cases highlighted in bold show an accuracy of less than 10%.

The calculated percentages of sediment deposition provide insights into the efficiency of sedimentation processes in the highlighted cases. Analyzing these values can help identify trends and inform future designs of sedimentation systems. It is essential to consider factors such as flow rates, sediment characteristics, and environmental conditions that may influence sediment deposition dynamics.

3.3. SPH Simulation on Debris Flow Impact

SPH has shown that it can predict occurrences and provide a good degree of agreement between observational data. Due to this, SPH is able to compute pressure, the hydrodynamic force acting on a static object, and the velocity of the two phases of debris flow. DualSPHysics v5.2.2. was used to simulate two cases with different geometries compared to previous cases, namely Case 1A and 1B.

For case 1A, the sizes of the width and height of the flume are doubled to 0.2 m width and 0.2 m height. The sediment size is increased to 0.2 width, 0.5 long, and 0.1 m height. The water level in the tank is raised to 200mm. A new geometry block is added to the deposition board and referred to as a building to see the force from the debris flow effect. The new geometry of the model is shown in Figure 2.

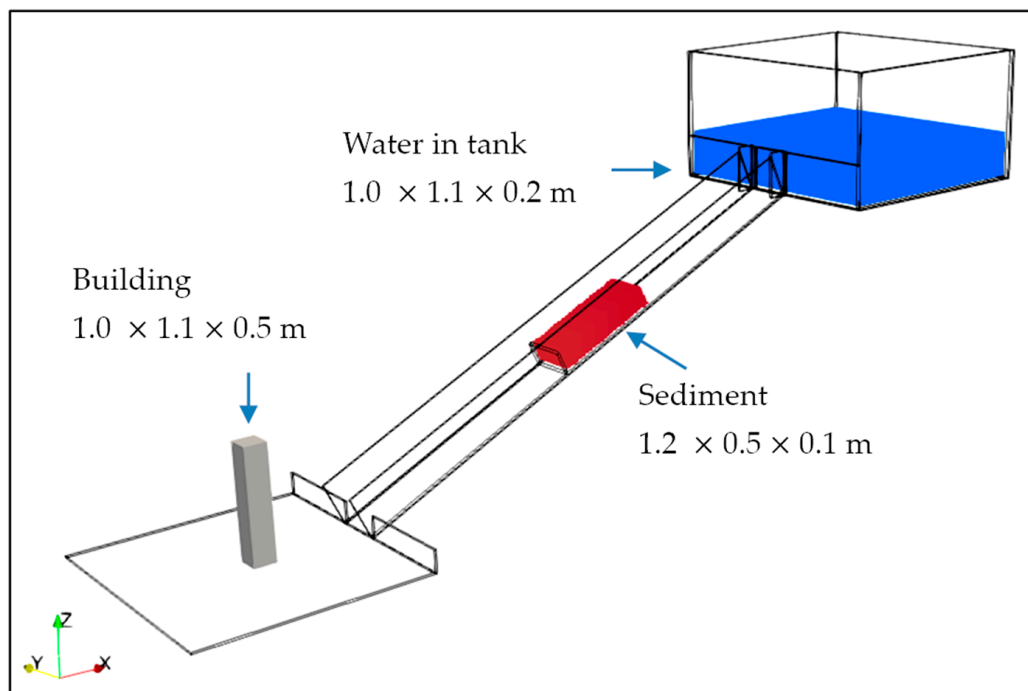


Figure 2. Geometry for debris flow impact model.

For Case 1B, the flume and sediment sizes are the same as in Case 1A. The only change to the model is the operation of the water gate, which is half open.

One monitoring point, Point A at (0.55, 0.65, 0.05) in the YXZ coordinate measured the velocity in front of the building block. The locations of these monitoring points are shown in Figure 3.

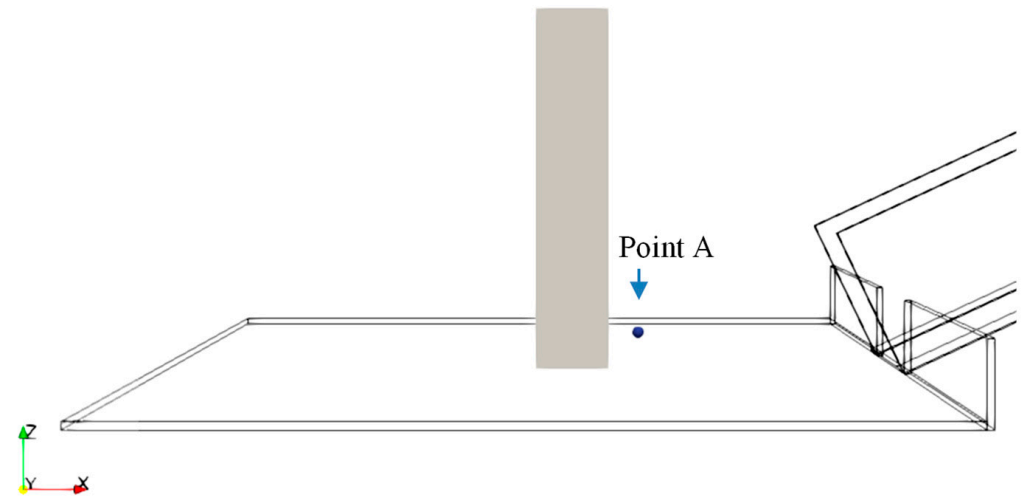


Figure 3. The measuring point in the model for Case 1A and 1B.

4. Result and Discussion

4.1. Case 1A

This case was operated at a water level of 200 mm and the gate was fully open for 5 s at a slope angle of 25°. The entire forces on the building block by fluid and sediment have been plotted in Figure 4. It can be seen in the figure that debris contacts the building block at 1.47 s. The maximum force value recorded is 55.2 N at 1.96 s and the mean is 5.45 N.

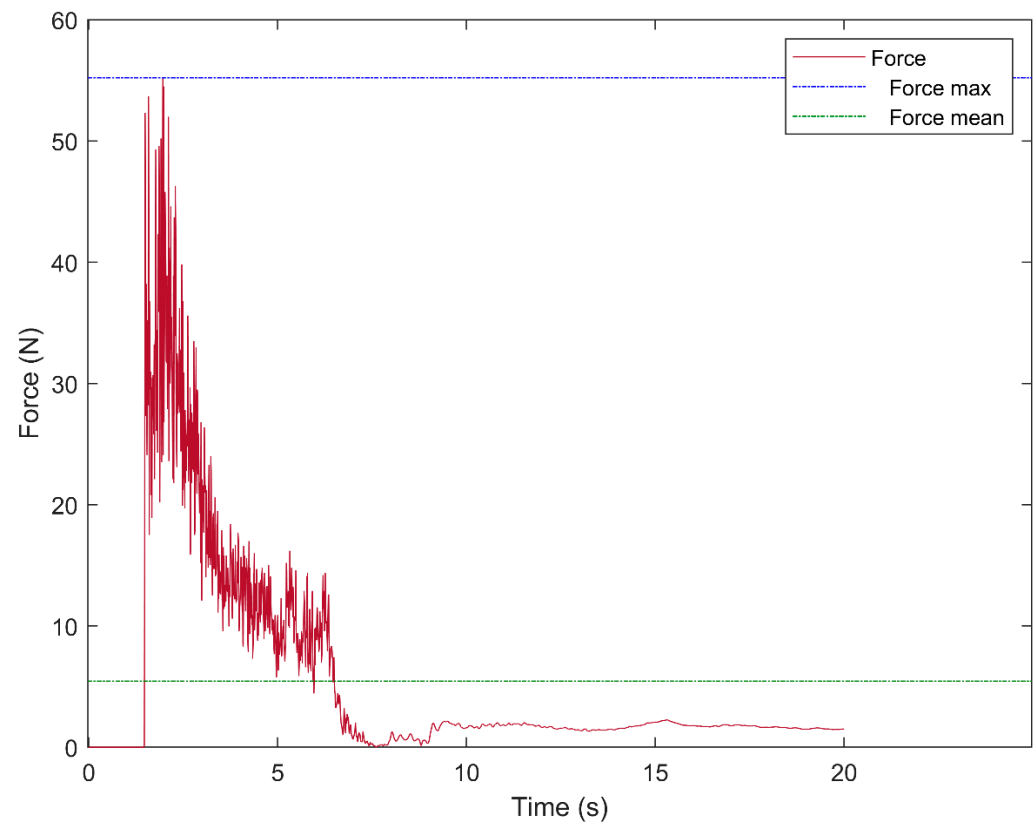


Figure 4. Plot of the forces on the building from Case 1A.

In Figure 5, the velocity for point A is plotted against time (second, s). The figure indicates that the debris flow reached 1.46 s, with a maximum recorded velocity of 3.44 cm/s at 3.46 s, and a mean velocity of 0.41 cm/s. The velocity diminished abruptly at 6.24 s and subsequently decreased gradually until 20 s due to the closing of the gate, resulting in a reduction in water flow until that point.

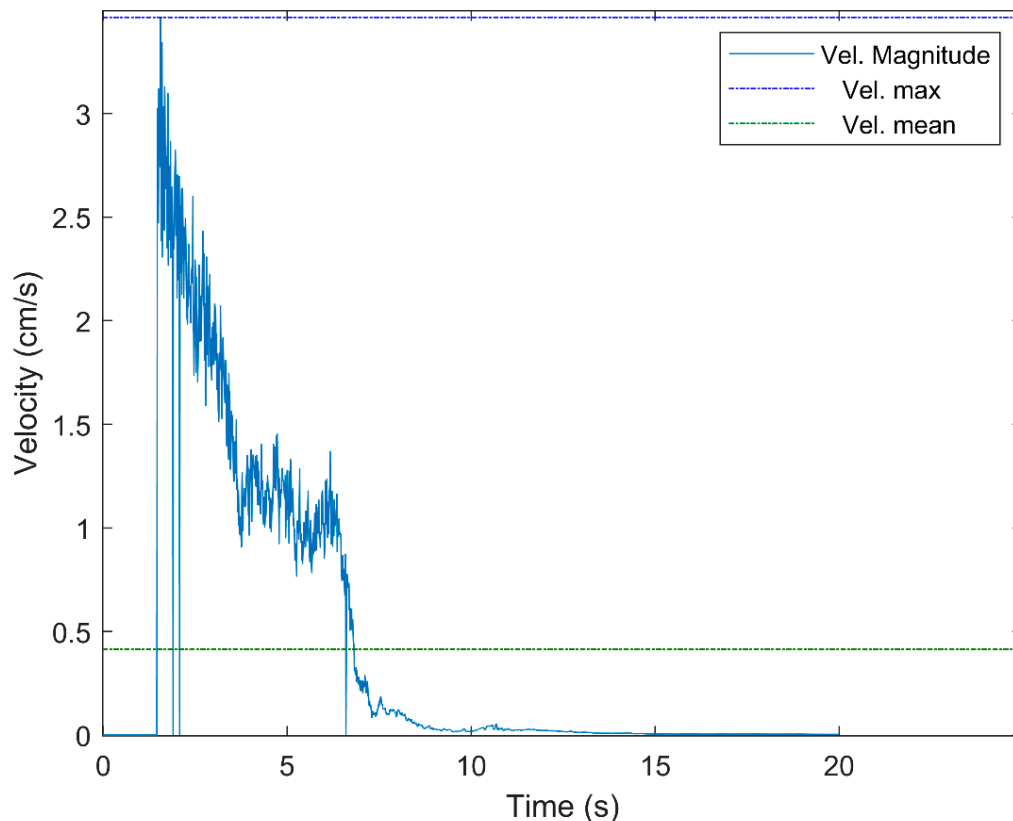


Figure 5. Velocity against time plotted on point A for Case 1.

This velocity magnitude graph shows three major stages; the acceleration stage after the mixture passes from the flume and reaches the monitoring point, the deceleration stage due to the viscosity of the mixture, and the propagation stage with a steady velocity. The pattern for velocity is approximately identical to force indicating that graph when velocity is high and force is high.

Figure 6 is a snapshot of the debris flow for Case 1A through the simulation. As shown in the figure, the water gate opens at $t = 0.10$ s, the fluid contacts the sediment at 0.56 s, then the two-phase mixture moves downstream to the deposition board. At $t = 1.34$ s, the mixture reaches the deposition and contacts the building block at $t = 1.46$ s. The mixture forms a flow shape at $t = 1.56$ s after the collision with the building block. The mixture starts to fill the deposition board at $t = 4.00$. At $t = 5.10$ s; the water gate closes; it can be seen that the mixture flow velocity starts to decrease, with the end result of the debris flow at $t = 20.00$ s.

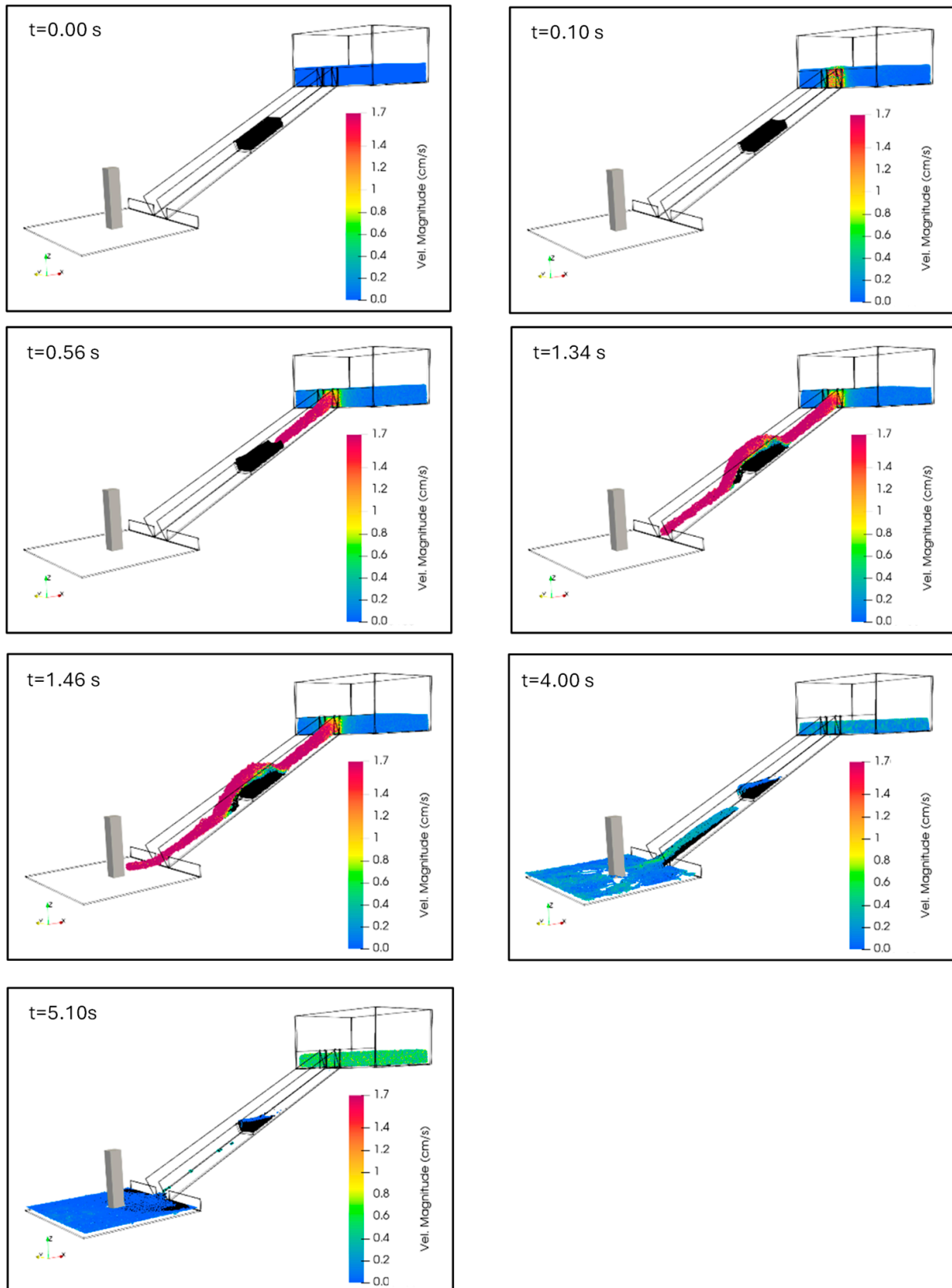


Figure 6. Velocity field of the simulation in different flow instants for Case 1A.

Figure 7 shows the debris pattern simulated by DualSPHysics on the deposition board. The sediment is represented by the black particles while the blue particles represent the water. A velocity reading of 0 cm/s indicates that the particles have stopped moving and have settled down. The results of the study showed that the shape exhibited a uniform runout pattern without channels on the fan and the building block in the middle facilitated deposition more effectively and evenly to the left and right. Consequently, the presence of an obstructive object, such as the building block, appears to play a significant role in the deposition pattern.

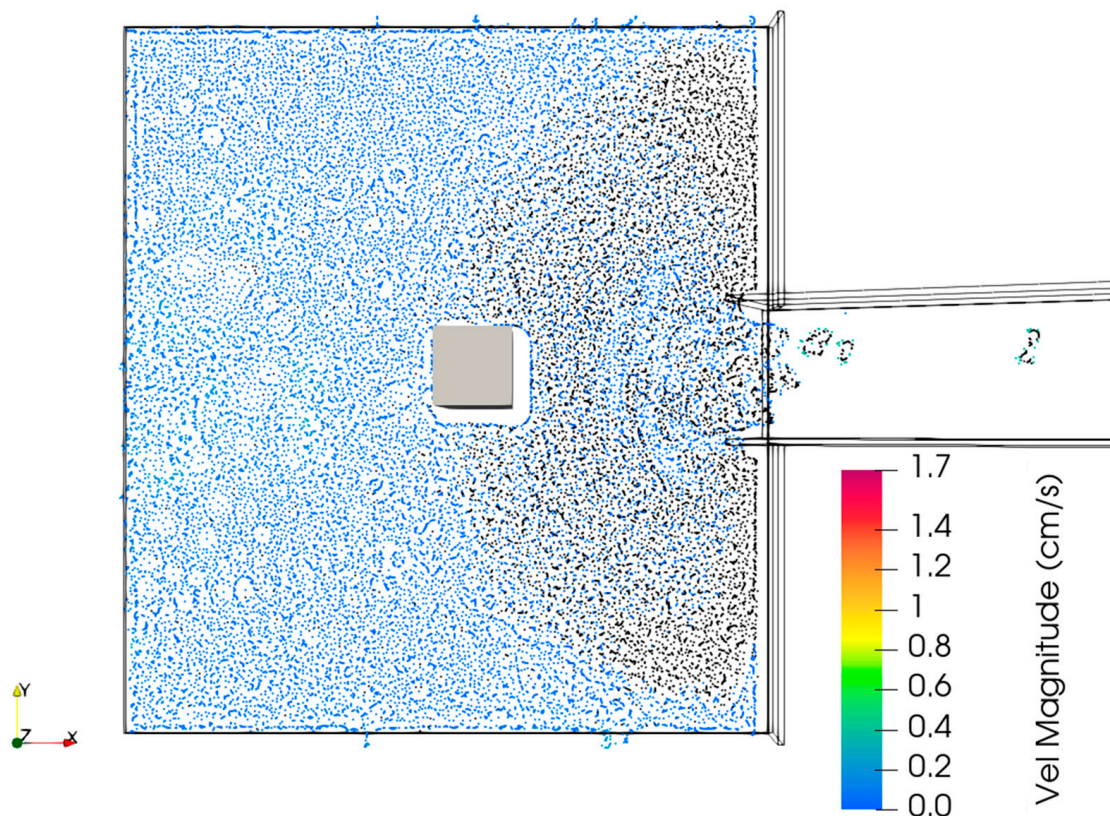


Figure 7. Simulation result of the debris deposition at $t = 20.00$ s for Case 1A.

4.2. Case 1B

This case was operated at a water level of 200 mm and the gate was half open for 5 s at a slope angle of 25° . The entire forces on the building block by fluid and sediment have been plotted in Figure 8. It can be seen in the figure that debris contacts the building block at 1.47 s. The maximum force value recorded is 47.3 N at 1.67 s and the mean is 3.24 N.

In Figure 9, the velocity for point A is plotted against time (s). From the figure, it can be seen that when the debris flow reaches 1.52 s, the maximum velocity recorded is 3.33 cm/s at 3.51 s and the mean velocity is 0.31 cm/s. The velocity decreases rapidly at 6.45 s then gradually decreases until 20 s because the gate is closed, and the water flow decreases until 20 s.

The velocity magnitude graph illustrates three main stages: acceleration once the mixture moves from the flume to the monitoring point, slowing caused by the mixture’s viscosity, and propagation at a constant velocity. The velocity pattern closely mirrors the force pattern, suggesting that when velocity is high and force is also high.

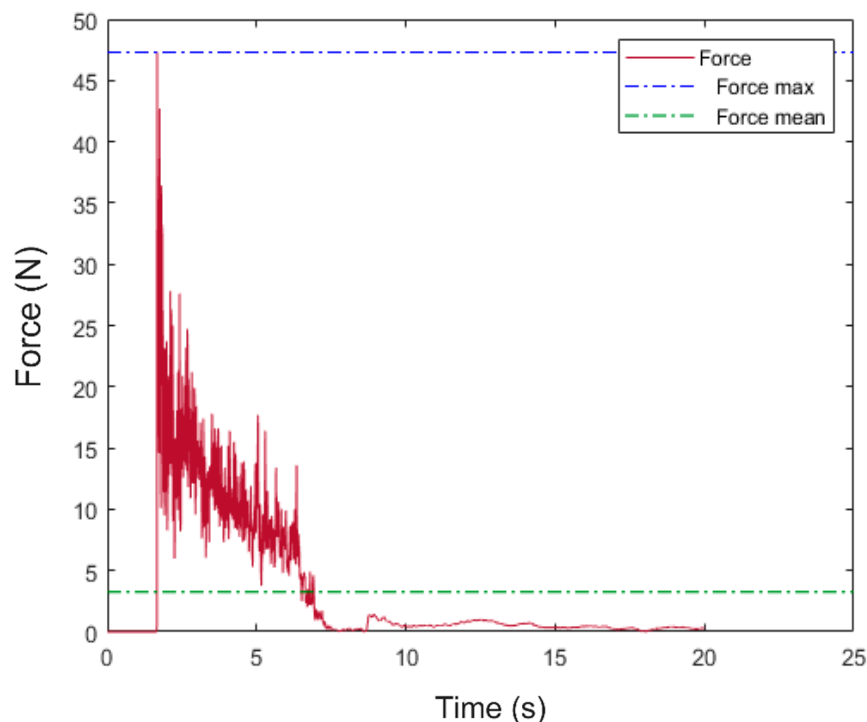


Figure 8. Plot of the forces on Building from Case 1B.

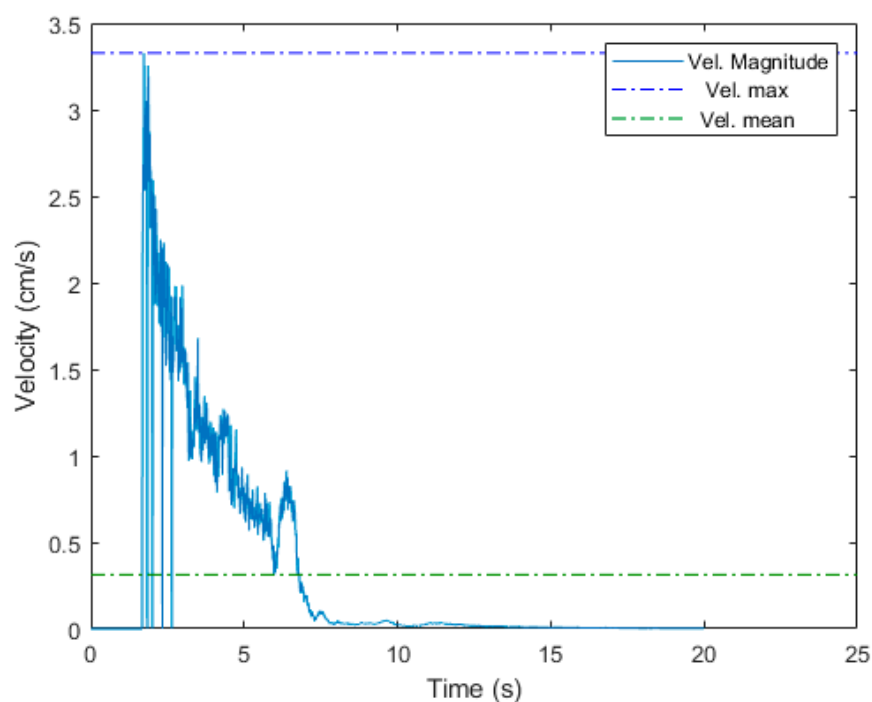


Figure 9. Velocity against time plotted on point A for Case 1B.

Figure 10 is a snapshot of the debris flow for Case 1B through the simulation. As shown in the figure, the water gate opens at $t = 0.10$ s, the fluid contacts the sediment at 0.60 s, and then the two-phase mixture moves downstream to the deposition board. At $t = 1.34$ s, the mixture reaches the deposition and contacts the building block at $t = 1.66$ s. The mixture forms a flow shape at $t = 1.80$ s after the collision with the building block. The mixture starts to fill the deposition board at $t = 4.00$. At $t = 5.10$ s, the water gate closes, it can be seen that the mixture flow velocity starts to decrease, with the end result of the debris flow at $t = 20.00$ s.

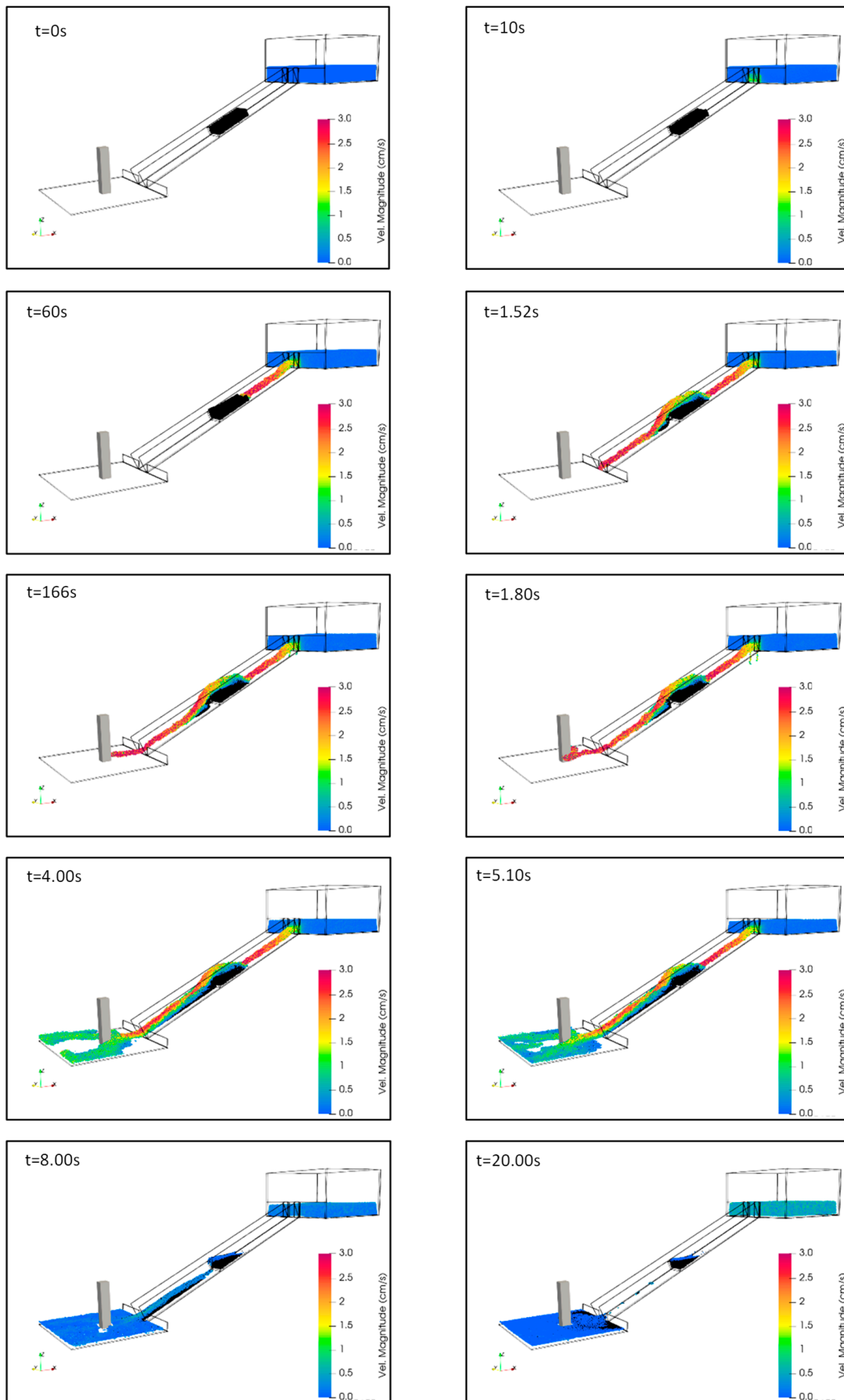


Figure 10. Velocity field of the simulation in different flow instants for Case 1B.

Figure 11 shows the debris pattern simulated by DualSPHysics on the deposition board. The black particles signify the sediment, whilst the blue particles denote the water. A velocity measurement of 0 cm/s signifies that the particles stopped moving and are now still. The study's results indicated that the shape displayed a consistent runout pattern free of channels, while the center building block boosted deposition more efficiently and uniformly to both the left and right. Thus, the existence of an obstructing object, like a building block, seems to significantly influence the deposition pattern.

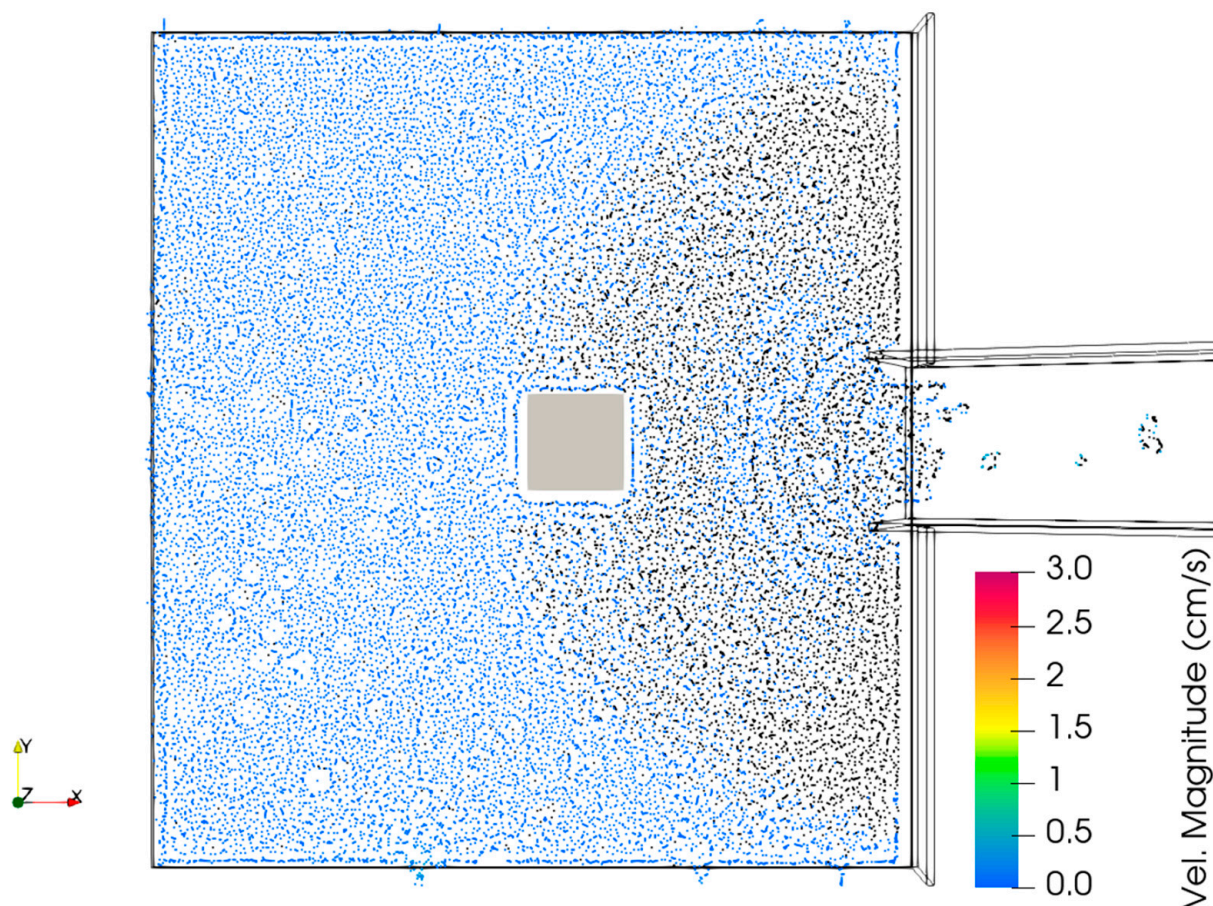


Figure 11. Simulation result of the debris deposition at $t = 20.00$ s for Case 1B.

4.3. Comparison Case 1A and 1B

This section compares the simulation data from the DualSPHysics model for both additional Case 1A and 1B. The comparison parameters can be seen in Table 4. The total elements for Case 1A and 1B are the same, which is 500,899 elements because no geometry has changed and only the operation of the gate is different. For Case 1A, the water gate will be fully opened in 5 seconds and Case 1B will be half opened in 5 s. The simulation runtime for Case 1A was 1 h 19 min and 33 s and 1 h 25 min and 55 s for Case 1B. Both cases are simulated for 20 s. This shows that operational changes in the model do not make a significant difference in simulation run time. The slight difference in runtime between the two cases may be attributed to the additional computational effort required to resolve the flow dynamics associated with the half-opened gate in Case 1B, which may introduce more complex flow patterns compared to a fully opened gate. However, the overall impact on simulation time remains minimal.

Table 4. Parameters for Case 1A and 1B.

Case	Slope Angle (°)	Water Level in Water Tank (m)	Water Gate Operation	Water Gate Open Time (s)	Total Elements	Simulation Runtime (HH:MM:SS)	Time of Simulation (s)
1A	25	0.2	Fully Open	5	500,899	1:19:33	20
1B	25	0.2	Half Open	5	500,899	1:25:55	20

Figure 12 shows the force from DualSPHysics for both cases. It can be seen in the Figure that debris hit the building block at 1.47 s for Case 1A and 0.19 s slower for Case 1B. The maximum force value recorded for Case 1A is 55.2 N at 1.96 s and the mean is 5.45 N. The maximum force value recorded for Case 1B is 47.3 N at 1.67 s and the mean is 3.24 N. The percentage difference in force mean value is 50.86%.

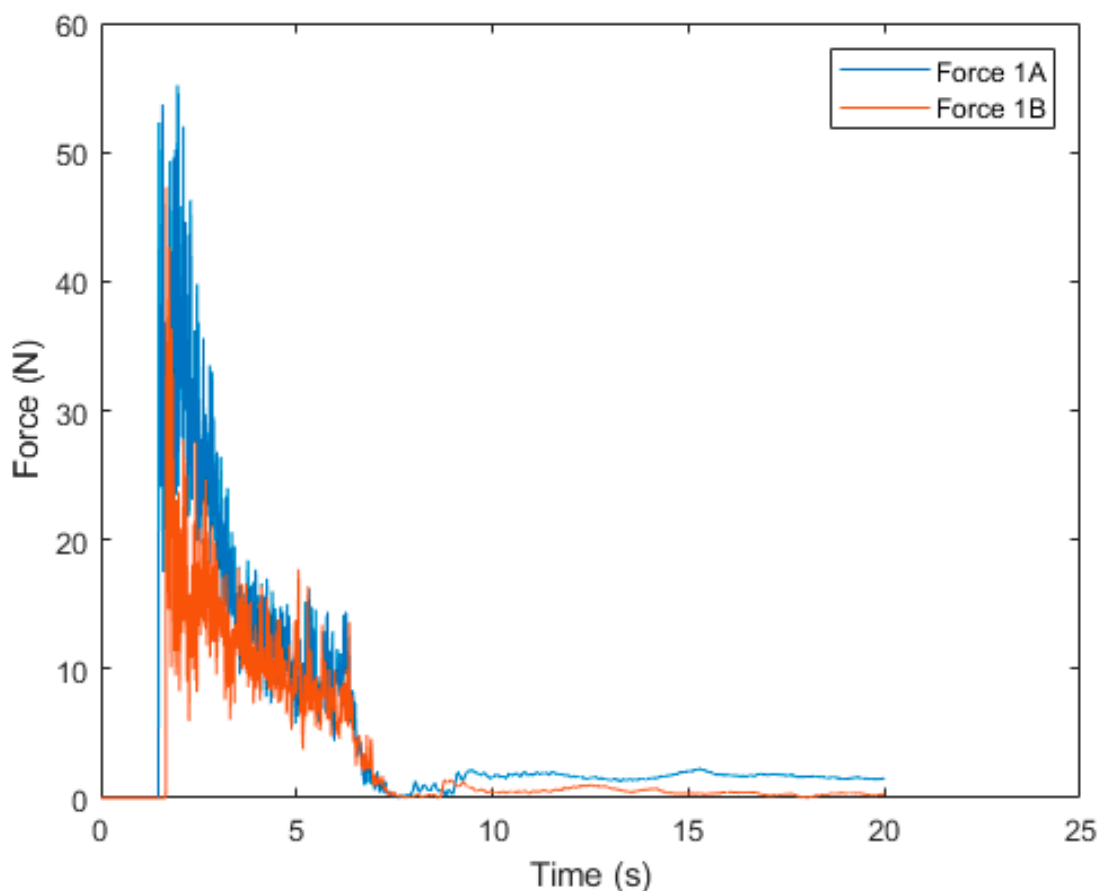


Figure 12. Plot of the force at building block for Case 1A and 1B in the DualSPHysics model.

From Figure 13, the velocity magnitude from the DualSPHysics model for both cases can be seen. The velocity magnitude in the Case 1B model follows the values from Case 1A very well. The velocity magnitude is very close, except for the large fluctuations at 5.57 until 6.40 s of the simulation. From Figure 13, it can be seen that the debris reached 1.46 s for Case 1A and 1.69 s for Case 1B, the maximum velocity recorded for Case 1A is 3.44 cm/s at 3.46 s and 3.33 cm/s for Case 1B. The mean velocity is 0.41 cm/s for Case 1A and 0.10 cm/s higher than Case 1B. The percentage difference in velocity magnitude mean value is 27.78%.

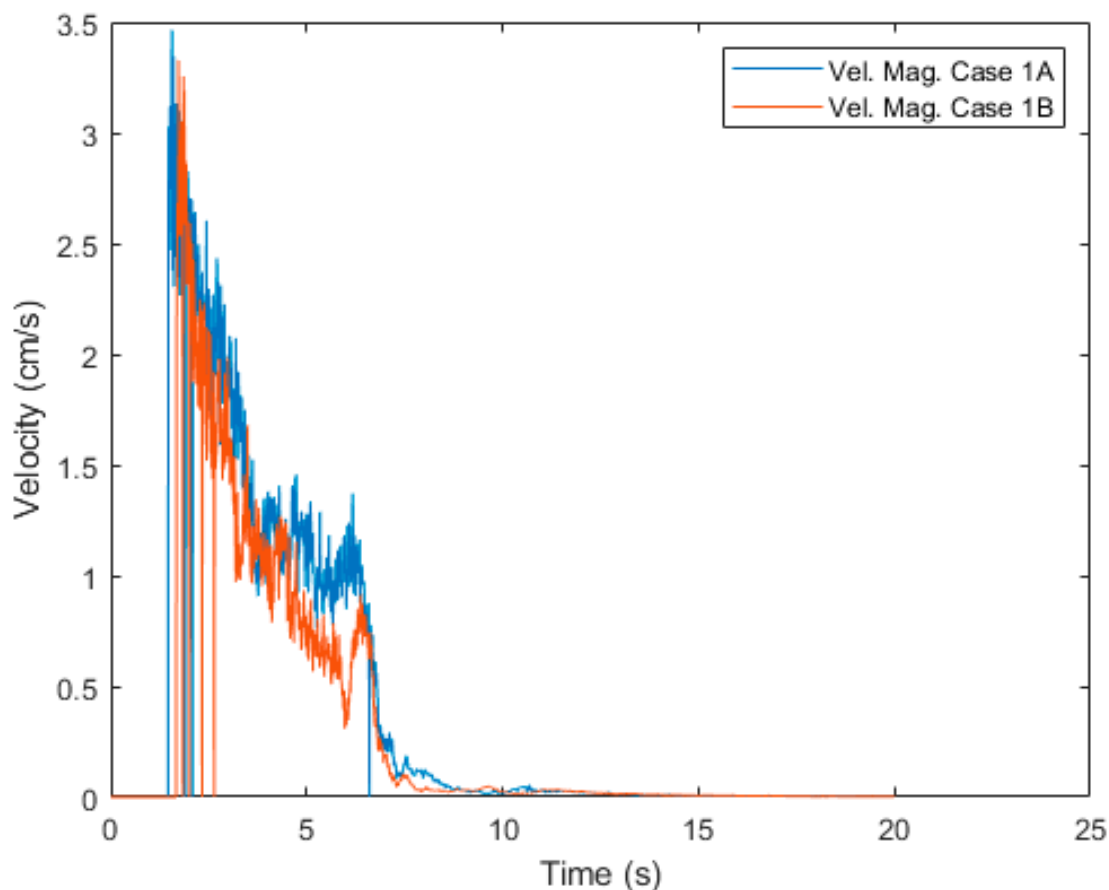


Figure 13. Plot of the velocity magnitude for Case 1A and 1B in the DualSPHysics model.

The velocity magnitude graph indicates that both scenarios undergo the same three primary stages previously described: the acceleration phase following the mixture's passage from the flume to the monitoring point, the deceleration phase attributed to the mixture's viscosity, and the propagation stage characterized by a constant velocity. The fluid volume influences velocity fluctuations, as evidenced by the velocity magnitude plots for Cases 1A and 1B in Figure 13.

Furthermore, the graphs have the same tendency of the force; the force mean value is reduced by more than half after the water gate is half opened. This is one more corroboration that the volume of the fluid plays a very important role in contributing to the changes in the velocity and force. The results comparison is made for both cases and can be seen in Table 5. The findings indicate a clear trend in the relationship between water gate operations and fluid dynamics. The significant reduction in mean force when the gate is half opened suggests that the volume of fluid directly affects the velocity and force exerted by the flow. The results align with the existing literature that emphasizes the importance of fluid volume in determining flow characteristics. As the volume of fluid decreases, the velocity and force also diminish, leading to more manageable flow conditions that can be beneficial in various engineering applications. The comparative analysis presented in Table 5 provides valuable insights for engineers and researchers in the field of hydraulic engineering.

Table 5. Results comparison for additional cases.

Case	Force			Vel. Magnitude		
	Max. (N)	Mean (N)	Mean Percentage Difference (%)	Max. (cm/s)	Mean (cm/s)	Mean Percentage Difference (%)
1A	55.2	5.45	50.86	3.44	0.41	27.78
1B	47.3	3.24		3.33	0.31	

5. Conclusions

In conclusion, this study demonstrates that while operational changes, specifically the rate of gate opening, do not significantly impact the simulation runtime in hydrodynamic models when the geometric configuration remains unchanged, such changes do have a notable effect on fluid dynamics. Furthermore, the effectiveness of hydrodynamic models in simulating fluid behavior under different operational scenarios is validated through a systematic approach involving twelve test cases. This approach not only provides a robust framework for future research and model refinement but also underscores the importance of establishing specific criteria to evaluate the reliability and validity of research findings, thereby maintaining the integrity of scientific inquiry. Notably, the study highlights the significant influence of water gate operations on fluid dynamics, with results indicating a reduction in mean force by more than half when the gate is half opened, emphasizing the critical role of fluid volume in these dynamics.

A quantitative assessment of the debris flow impact force was necessary in order to reduce the human and property damage caused by debris flows. Impact force considerably influences the degree of damage. However, due to work limitations, this study is only able to simulate debris flow runout and does not account for impact force. In actual situations, the maximum impact force (5520 N) can be 100 times greater compared to model values (55.2 N). Imagine that during the event, structures at the deposition area were impacted by an impact force that was 100 times greater. This study highlights the critical need for accurate assessments of debris flow impact forces to inform risk management and mitigation strategies. The observed discrepancies between simulated and actual forces necessitate the development of more sophisticated models that can better predict the behavior of debris flows and their potential impacts.

Future research should focus on integrating impact force assessments into debris flow simulations to enhance the reliability of predictions and improve safety measures for affected communities and the environment. Understanding the potential impact forces on both human settlements and natural ecosystems can inform the design and retrofitting of structures in debris flow-prone areas. Additionally, this knowledge can guide the protection of critical habitats, minimizing the disruption to local biodiversity and mitigating environmental degradation. Engineering solutions, such as reinforced structures, barriers, and early warning systems, can significantly reduce the risk of damage, environmental harm, and loss of life. Furthermore, sustainable land-use planning and ecological restoration projects should be considered to strengthen natural defenses, such as vegetation buffers, that can reduce debris flow velocity. Community education, preparedness programs, and ecosystem management initiatives are also vital for enhancing public awareness of debris flow hazards and promoting timely evacuation procedures while safeguarding the surrounding environment. Moreover, this event may have caused significant harm, financial losses, environmental damage, and even fatalities.

Author Contributions: Conceptualization, M.K.A.W. and M.R.R.M.A.Z.; methodology, M.K.A.W. and N.A.R.; software, M.K.A.W. and M.A.A.; validation, N.A.R.; formal analysis, M.K.A.W.; investigation, M.K.A.W., N.A.R. and M.A.A.; resources, M.K.A.W.; data curation, M.K.A.W.; writing—original draft preparation, M.K.A.W.; writing—review and editing, M.K.A.W.; visualization, M.K.A.W.; supervision, M.R.R.M.A.Z.; project administration, M.R.R.M.A.Z., N.A.R. and M.A.A.; funding acquisition, M.R.R.M.A.Z. All authors have read and agreed to the published version of the manuscript.

Funding: This research was supported by the Ministry of Higher Education Malaysia under the Highest Institution Center of Excellence (HICOE) research grant (311.PREDAC.4403901) and the Ministry of Higher Education Malaysia for Fundamental Research Grant Scheme with the following project code: FRGS/1/2016/TK01/USM/02/4.

Institutional Review Board Statement: Not applicable.

Informed Consent Statement: Not applicable.

Data Availability Statement: Not applicable.

Acknowledgments: The authors extend their sincere gratitude to the Ministry of Higher Education Malaysia for its support through the Highest Institution Center of Excellence (HICOE) initiative.

Conflicts of Interest: The authors declare no conflicts of interest.

References

1. Takahashi, T. A Review of Japanese Debris Flow Research. *Int. J. Eros. Control Eng.* **2009**, *2*, 1–14. [[CrossRef](#)]
2. Zhou, G.D.; Law, R.P.H.; Ng, C.W.W. The mechanisms of debris flow: A preliminary study. In Proceedings of the 17th International Conference on Soil Mechanics and Geotechnical Engineering, Alexandria, Egypt, 5–9 October 2009; Volume 2, pp. 1570–1573. [[CrossRef](#)]
3. Mohd Arif Zainol, M.R.R.; AWahab, M.K. Hydraulic Physical Model of Debris Flow for Malaysia Case Study. *IOP Conf. Ser. Mater. Sci. Eng.* **2018**, *374*. [[CrossRef](#)]
4. Tiranti, D.; Crema, S.; Cavalli, M.; Deangeli, C. An Integrated Study to Evaluate Debris Flow Hazard in Alpine Environment. *Front. Earth Sci.* **2018**, *6*, 1–14. [[CrossRef](#)]
5. Muhammad, N.S.; Julien, P.Y.; Salas, J.D. Probability Structure and Return Period of Multiday Monsoon Rainfall. *J. Hydrol. Eng.* **2016**, *21*, 1. [[CrossRef](#)]
6. Rahman, H.A.; Mapjabil, J. Landslides Disaster in Malaysia: An Overview. *Heal. Environ. J.* **2017**, *8*, 58–71.
7. Wahab, M.K.; Mohd Arif Zainol, M.R.R.; Ikhsan, J.; Zawawi, M.H.; Abas, M.A.; Mohamed Noor, N.; Abdul Razak, N.; Bhardwaj, N.; Mohamad Faudzi, S.M. Smoothed particle hydrodynamics simulation of debris flow on deposition area. *Nat. Hazards* **2024**, *120*, 12107–12136. [[CrossRef](#)]
8. Joe, E., Jr.; Tongkul, F.; Roslee, R. Engineering Properties of Debris Flow Material At Bundu Tuhan, Ranau, Sabah, Malaysia. *Pakistan J. Geol.* **2018**, *2*, 22–26. [[CrossRef](#)]
9. Kasim, N.; Taib, K.A.; Mukhlisin, M.; Kasa, A. Triggering Mechanism and Characteristic of Debris Flow in Peninsular Malaysia. *Am. J. Engineering Res.* **2016**, *5*, 112–119.
10. Khairi, M.A.W.; Rozainy, M.R.; Ikhsan, J. Smoothed Particle Hydrodynamics Simulation for Debris Flow: A Review. *IOP Conf. Ser. Mater. Sci. Eng.* **2020**, *864*, 012045. [[CrossRef](#)]
11. Liu, K.F.; Huang, M.C. Numerical simulation of debris flows. *Proc. Int. Conf. Offshore Mech. Arct. Eng.—OMAE* **2010**, *6*, 375–382. [[CrossRef](#)]
12. Chang, T.C.; Wang, Z.Y.; Chien, Y.H. Hazard assessment model for debris flow prediction. *Environ. Earth Sci.* **2010**, *60*, 1619–1630. [[CrossRef](#)]
13. Li, M.; Jiang, Y.; Yang, T.; Huang, Q.; Qiao, J.; Yang, Z. Early warning model for slope debris flow initiation. *J. Mt. Sci.* **2018**, *15*, 1342–1353. [[CrossRef](#)]
14. Vargas-Cuervo, G.; Rotigliano, E.; Conoscenti, C. Prediction of debris-avalanches and -flows triggered by a tropical storm by using a stochastic approach: An application to the events occurred in Mocoa (Colombia) on 1 April 2017. *Geomorphology* **2019**, *339*, 31–43. [[CrossRef](#)]
15. Zhou, J.W.; Cui, P.; Yang, X.G.; Su, Z.M.; Guo, X.J. Debris flows introduced in landslide deposits under rainfall conditions: The case of Wenjiagou gully. *J. Mt. Sci.* **2013**, *10*, 249–260. [[CrossRef](#)]
16. Chen, S.C.; Wu, C.Y. Debris flow disaster prevention and mitigation of non-structural strategies in Taiwan. *J. Mt. Sci.* **2014**, *11*, 308–322. [[CrossRef](#)]

17. Lay, U.S.; Pradhan, B. Identification of debris flow initiation zones using topographic model and airborne laser scanning data. *Lect. Notes Civ. Eng.* **2019**, *9*, 915–940. [[CrossRef](#)]
18. Pradhan, B.; Bakar, S.B.A. *Debris Flow Source Identification in Tropical Dense Forest Using Airborne Laser Scanning Data and Flow-R Model BT—Laser Scanning Applications in Landslide Assessment*; Pradhan, B., Ed.; Springer International Publishing: Cham, Switzerland, 2017; pp. 85–112.
19. Yosuke, Y.; Rozainy, M.A.Z.M.R.; Taku, M.; Tamotsu, T.; Kaoru, T. Experimental study of debris particles movement characteristics at low and high slope. *J. Glob. Environ. Eng.* **2012**, *17*, 9–18.
20. Borga, M.; Stoffel, M.; Marchi, L.; Marra, F.; Jakob, M. Hydrogeomorphic response to extreme rainfall in headwater systems: Flash floods and debris flows. *J. Hydrol.* **2014**, *518*, 194–205. [[CrossRef](#)]
21. Naqvi, D.K.C.M.W.; Hu, L. A Case Study and Numerical Modeling of Post-Wildfire Debris Flows in Montecito, California. *Water* **2024**, *16*, 1285. [[CrossRef](#)]
22. Kean, J.W.; Staley, D.M.; Lancaster, J.T.; Rengers, F.K.; Swanson, B.J.; Coe, J.A.; Hernandez, J.L.; Sigman, A.J.; Allstadt, K.E.; Lindsay, D.N. Inundation, Flow Dynamics, and Damage in the 9 January 2018 Montecito Debris-Flow Event, California, USA: Opportunities and Challenges for Post-Wildfire Risk Assessment. *Geosphere* **2019**, *15*, 1140–1163. [[CrossRef](#)]
23. Tuckett, Q.M.; Koetsier, P. Mid- And Long-Term Effects of Wildfire and Debris Flows on Stream Ecosystem Metabolism. *Freshw. Sci.* **2016**, *35*, 445–456. [[CrossRef](#)]
24. Parise, M.; Cannon, S.H. Wildfire Impacts on the Processes That Generate Debris Flows in Burned Watersheds. *Nat. Hazards* **2011**, *61*, 217–227. [[CrossRef](#)]
25. Zhang, J.; Guo, Z.; Wang, D.; Qian, H. The Quantitative Estimation of the Vulnerability of Brick and Concrete Building Impacted by Debris Flow. *Nat. Hazards Earth Syst. Sci. Discuss.* **2015**, *3*, 5015–5044. [[CrossRef](#)]
26. Ciurean, R.L.; Hussin, H.; van Westen, C.J.; Jaboyedoff, M.; Nicolet, P.; Chen, L.; Frigerio, S.; Glade, T. Multi-Scale Debris Flow Vulnerability Assessment and Direct Loss Estimation of Buildings in the Eastern Italian Alps. *Nat. Hazards* **2016**, *85*, 929–957. [[CrossRef](#)]
27. Nicolae, A.F.; Deák, G.; Tudor, G.; Cirstinoiu, C.T.; Zamfir, A.S.; Uritescu, B.; Georgescu, L.; Ghita, G.; Raischi, M.; Daescu, A.I.; et al. Comparative analysis on water velocity distribution in the context of riverbed morphology changes and discharge variation. *J. Environ. Prot. Ecol.* **2017**, *18*, 1649–1657.
28. Hu, K.; Cui, P.; Zhang, J.Q. Characteristics of Damage to Buildings by Debris Flows on 7 August 2010 in Zhouqu, Western China. *Nat. Hazards Earth Syst. Sci.* **2012**, *12*, 2209–2217. [[CrossRef](#)]
29. Bugnion, L.; McArdell, B.W.; Bartelt, P.; Wendeler, C. Measurements of Hillslope Debris Flow Impact Pressure on Obstacles. *Landslides* **2011**, *9*, 179–187. [[CrossRef](#)]
30. Luo, H.; Zhang, L.M.; He, J.; Yin, K. Reliability-Based Formulation of Building Vulnerability to Debris Flow Impacts. *Can. Geotech. J.* **2022**, *59*, 40–54. [[CrossRef](#)]
31. Kang, H.-G.; Kim, Y.-T. Physical Vulnerability Function of Buildings Impacted by Debris Flow. *Korean Soc. Hazard Mitig.* **2014**, *14*, 133–143. [[CrossRef](#)]
32. Liu, X.; Wang, F.; Nawnit, K.; Lv, X.; Wang, S. Experimental study on debris flow initiation. *Bull. Eng. Geol. Environ.* **2020**, *79*, 1565–1580. [[CrossRef](#)]
33. Zhuang, J.; Cui, P.; Peng, J.; Hu, K.; Iqbal, J. Initiation process of debris flows on different slopes due to surface flow and trigger-specific strategies for mitigating post-earthquake in old Beichuan County, China. *Environ. Earth Sci.* **2013**, *68*, 1391–1403. [[CrossRef](#)]
34. Yamashiki, Y.; Rozainy, M.A.Z.M.R.; Matsumoto, T.; Takahashi, T.; Takara, K. Particle Routing Segregation of Debris Flow Mechanisms Near the Erodible Bed. *APCBEE Procedia* **2013**, *5*, 527–534. [[CrossRef](#)]
35. Dai, Z.; Wang, F.; Huang, Y.; Song, K.; Iio, A. SPH-based numerical modeling for the post-failure behavior of the landslides triggered by the 2016 Kumamoto earthquake. *Geoenvironmental Disasters* **2016**, *3*, 24. [[CrossRef](#)]
36. Liu, G.-R.; Liu, M.B. *Smoothed Particle Hydrodynamics: A Meshfree Particle Method*; World Scientific Publishing Co. Pte. Ltd: Singapore, 2010.
37. Liu, M.B.; Liu, G. Smoothed particle hydrodynamics (SPH): An overview and recent developments. *Arch. Comput. methods Eng.* **2010**, *17*, 25–76. [[CrossRef](#)]
38. Gomez-Gesteira, M.; Rogers, B.D.; Crespo, A.J.C.; Dalrymple, R.A.; Narayanaswamy, M.; Dominguez, J.M. SPHysics—development of a free-surface fluid solver—Part 1: Theory and formulations. *Comput. Geosci.* **2012**, *48*, 289–299. [[CrossRef](#)]
39. Li, B.; Fang, Y.; Li, Y.; Zhu, C. Dynamics of Debris Flow-Induced Impacting Onto Rigid Barrier With Material Source Erosion-Entrainment Process. *Front. Earth Sci.* **2023**, *11*, 1132635. [[CrossRef](#)]
40. Li, B.; Wang, C.; Li, Y.; Zhang, S. Dynamic Response Study of Impulsive Force of Debris Flow Evaluation and Flexible Retaining Structure Based on SPH-DEM-FEM Coupling. *Adv. Civ. Eng.* **2021**, *2021*, 098250. [[CrossRef](#)]
41. Zhao, H.; Yao, L.; You, Y.; Wang, B.; Zhang, C. Experimental Study of the Debris Flow Slurry Impact and Distribution. *Shock Vib.* **2018**, *2018*, 460362. [[CrossRef](#)]

42. Yang, X.F.; Peng, S.L.; Liu, M.B. A new kernel function for SPH with applications to free surface flows. *Appl. Math. Model.* **2014**, *38*, 3822–3833. [[CrossRef](#)]
43. Zhang, Z.; Zhang, W.; Zhai, Z.J.; Chen, Q.Y.; Zhai, Z.J.; Chen, Q.Y. Evaluation of Various Turbulence Models in Predicting Airflow and Turbulence in Enclosed Environments by CFD: Part 2—Comparison with Experimental Data from Literature. *HVAC&R Res.* **2007**, *13*, 871–886.
44. Tudor, G.; György, D.; Cirstinoiu, C.; Raischi, M.; Danalache, T.; Cornateanu, G.; Bratfanof, E. Transboundary River Hydrodynamic Conditions Assessment in Sustainable Development Context. A Case Study of Danube River: Chilia Branch—Bystroe Channel Area. *IOP Conf. Ser. Earth Environ. Sci.* **2020**, *616*, 012072. [[CrossRef](#)]

Disclaimer/Publisher’s Note: The statements, opinions and data contained in all publications are solely those of the individual author(s) and contributor(s) and not of MDPI and/or the editor(s). MDPI and/or the editor(s) disclaim responsibility for any injury to people or property resulting from any ideas, methods, instructions or products referred to in the content.